Catalysis Letters Vol. 100, Nos. 3–4, April 2005 (© 2005)
DOI: 10.1007/s10562-004-3461-6

Skeletal isomerization of octadecane on bifunctional ZSM-23 zeolite catalyst

Ward Huybrechts[a], Gina Vanbutsele[a], Kristof J. Houthoofd[a], Fabrice Bertinchamps[b], C. S. Laxmi Narasimhan[d], Eric M. Gaigneaux[b], Joris W. Thybaut[d], Guy B. Marin[d], Joeri F. M. Denayer[c], Gino V. Baron[c], Pierre A. Jacobs[a], and Johan A. Martens[a,*]

[a]*Centrum voor Oppervlaktechemie en Katalyse, Katholieke Universiteit Leuven, Kasteelpark Arenberg 23, B-3001 Leuven, Belgium*
[b]*Unité de Catalyse et chimie des matériaux divisés, Université Catholique de Louvain, Croix du Sud, 2 Bte 17, B-1348 Louvain-la-Neuve, Belgium*
[c]*Dienst Chemische Ingenieurstechniek, Vrije Universiteit Brussel, Pleinlaan 2, B-1050 Brussel, Belgium*
[d]*Laboratorium voor Petrochemische Techniek, Universiteit Gent, Krijgslaan 281, B-9000 Gent, Belgium*

Received 1 July 2004; accepted 11 December 2004

Octadecane was isomerized over three different Pt/H-ZSM-23 samples. The distributions of methylheptadecane and dimethylheptadecane skeletal isomers obtained on the Pt/ZSM-23 samples were very similar. Positional isomer distributions are fingerprints of the zeolite framework structure. The independence of skeletal isomer distributions from Al-gradients and particle size constitutes a strong argument in favor of pore-mouth catalysis.

KEY WORDS: isodewaxing; *n*-alkanes; ZSM-23 zeolite; skeletal isomerization; octadecane.

1. Introduction

The introduction of branchings in the carbon skeleton of long *n*-alkanes contained in paraffinic petroleum fractions results in improved bulk physical properties such as pour point and freezing point lowering. For obtaining the desired branching while limiting the undesired cracking of the molecules, catalytic hydroconversion processes over bifunctional zeolites with tubular 10-ring pore system can be used [1]. Platinum-plated, proton exchanged aluminosilicate zeolites with TON framework type such as Pt/ZSM-22 and Pt/Theta-1 are representative of this family of zeolite materials. Several studies were devoted to the skeletal isomerization of long *n*-alkanes on TON type zeolites [2–9]. With these zeolite catalysts, the branchings are methyl groups, generated at very specific carbon positions along the alkane chains as revealed in conversions of model *n*-alkanes with carbon numbers up to *n*-C_{24}. In the monobranched isomers obtained out of *n*-alkanes on TON type zeolites, the preferred methylbranching positions are C_2 and, with long chains, C_5–C_{12} [6,9]. In the preferred dimethylbranched skeletal isomers, the methyl side chains are located at far apart positions along the main chain. The minimum spacing between the branchings is dependent on the chain length. For the 2,*m*-dMe–C_{n-2} fraction, it varies from three carbon atoms for short C_n chains, to five carbon atoms for long C_n chains. In the most favored skeletal isomers of the 3,*n*-dMe–C_{n-2} type, the two branchings are spaced by at least 4 or 5 carbons [7].

There is general agreement in literature that the suppression of formation of dimethylbranched skeletal isomers with quaternary carbon atoms and with proximate methyl groups is a manifestation of transition state shape selectivity [2,6,10,11]. The visions diverge, however, on the mechanism responsible for the peculiar selectivity patterns among the monobranched and dibranched positional isomers. One interpretation is that the *n*-alkanes undergo branching rearrangements inside the pores. The relative diffusivities of the different positional isomers are different and the product is enriched with the fastest diffusing isomers. Arguments in favor of such product shape selectivity are mainly based on computer simulations of adsorption and diffusion of the different skeletal isomers in a molecular model of the zeolite channel [9,10,12,13]. Webb III *et al.* [12,13] calculated diffusion constants and activation energies for diffusion of linear and branched alkanes using molecular dynamics simulations. The TON channel has every 0.5 nm a shallow lobe in its wall. The lobes alternate on two opposite sides of the channel. Methylbranched alkanes position themselves preferentially with their methyl branch inside such lobe. 2-Methylbranched alkanes have a symmetric tail of two methyl groups attached to the carbon atom at the C2 position. Simultaneous positioning of both of these methyl groups inside lobes is not possible. The 3-methylbranched molecules have an asymmetric tail. At the potential minimum, the methyl groups of methylbranched molecules are positioned in a lobe. As a consequence the hop

* To whom correspondence should be addressed.
E-mail: Johan.Martens@agr.kuleuven.ac.be

frequency of 2-methylbranched molecules is higher than of 3-methylbranched molecules. This is the basis for the suggestion that the preferential formation of 2-methylbranched molecules over 3-methylbranched molecules is a manifestation of product diffusion shape selectivity. The zeolite topology has a strong influence on relative diffusivities of methylalkanes. For *n*-methylnonanes, the minimum diffusivity estimated with molecular dynamics simulations is at C-atom position 2, 3 and 4 in FER, EUO and TON, respectively [12]. Sastre *et al*. [9] simulated the diffusion of seven carbon alkane isomers in TON channels and concluded that monomethylbranched isomers diffuse through the pores, whereas 2,3-dimethylbutene could not. Similar approaches and CBMC calculations led other authors to propose that the selectivity among the dimethylbranched isomers is also dominated by the relative diffusivities [10]. Schenk *et al*. [14] calculated the free energy of formation of various dimethylbranched alkane isomers in TON type channels. Isomers with a spacing of the methyl groups matching with that of the lobes along the pore were estimated to diffuse slower than isomers the branching of which fitted less well with the arrangement of the lobes. Accordingly, 2,6- and 2,10-dimethylalkanes were proposed to be less abundant products compared to 2,7-, 2,8- and 2,9-dimethylalkanes. Furthermore, the computer model predicted formation of 3,8-, 3,9- and 3,10-dimethylalkanes to be more abundantly formed than 3,7-dimethylalkanes. These predictions diverge considerably from experimentally obtained product distributions [7].

Experimental investigations led to an explanation of the peculiar reaction selectivity patterns on ZSM-22 by invoking pore mouth and key–lock catalysis [5–7]. The product patterns can be explained as follows. The long *n*-alkane reacts when it is adsorbed partly inside, partly outside the pore (pore mouth), or with both tails inside two different pores (key–lock). The methyl groups, generated by contraction of the main chain by one carbon atom, are formed preferentially in the first lobe of the pore, where desorption is least sterically hindered.

Further evidence for the pore-mouth-mechanism on ZSM-22 came from adsorption measurements on open and closed ZSM-22 [15]. These measurements of adsorption equilibria of alkane vapors on ZSM-22 confirmed that under reaction conditions *iso*-alkanes do not enter micropores of ZSM-22, while *n*-alkanes do. Branched C5–C9 alkanes penetrate inside ZSM-22 crystals only when applied in liquid phase but not in vapor phase relevant to the hydroisomerization experiments run in the laboratory [16]. A fundamental kinetic model based on pore-mouth and key–lock catalysis has been developed and successfully implemented for the description of the shape-selective hydroconversion on Pt/H-ZSM-22 [17].

ZSM-22 and ZSM-23 are related zeolite structures with TON and MTT topology, respectively. The MTT framework can be considered to be a recurrently twinned variant of the TON framework [18]. The 10-ring pores in both topologies are undulated, but the undulation pattern is different. In materials with MTT topology, the cross section has the shape of a teardrop, with maximum and minimum free diameters of 0.52 and 0.45 nm, respectively. In the TON structure types, the 10-rings delineating the pores have an elliptical shape, with maximum and minimum widths of 0.57 and 0.46 nm, respectively. Consequently, the architecture of the pores and pore mouths of TON and MTT are substantially different.

The behavior of ZSM-23 in alkane adsorption and conversion is less documented. Branched C5–C9 alkanes provided as vapor or liquid have no access to the intracrystaline void spaces of ZSM-23 zeolite [16]. In decane [19,20] and dodecane [21] hydroisomerization on Pt/ZSM-23, the product features typical of ZSM-22 were present, but less pronounced.

We converted three samples of ZSM-23 differing with respect to Al content and distribution, microporosity and particle size into bifunctional catalysts and performed octadecane isomerization experiments in order to find out how the differences in physico-chemical properties would be reflected in the skeletal isomerization of a very long *n*-alkane.

2. Experimental

2.1. Zeolite materials

The properties of the three ZSM-23 samples and reference ZSM-22 sample are listed in table 1. ZSM-23[24] was kindly provided by R. van Veen. ZSM-23[44] was prepared following a recipe from Ernst *et al*. [20]. ZSM-23[55] was prepared according to Example 2 in USP 4,490,342. The morphology of the ZSM-23[24] and ZSM-23[44] samples is quite similar as revealed by SEM (figure 1). Lath shaped crystals predominate. In ZSM-23[24] and -[44] these laths are isolated; in ZSM-23[55] the majority of them are aggregated into differently sized elongated bodies. Compared to the reference ZSM-22 material, prepared following a recipe from Ernst *et al*. [22] and having a bulk Si/Al ratio of 54, the crystals are much wider and a little shorter.

The zeolite powders were calcined and ammonium exchanged in order to reduce the Na_2O content to below 0.04 wt%. The porosity was characterized using nitrogen adsorption at −196 °C using an Omnisorp 100 instrument from Coulter. Micropore volumes and external surface area's were derived from the isotherms using the *t*-plot method (table 1). ^{27}Al MAS NMR spectra were recorded with a Bruker Avance DRX400 spectrometer (9.4 *T*). A number of 12,000 scans were accumulated with a recycle delay of 100 ms. The sample holders were spun at 20 kHz. In all investigated samples aluminum was in tetrahedral co-ordination. Octahe-

Table 1
Properties of ZSM-23 and ZSM-22 samples

	ZSM-23[24]	ZSM-23[44]	ZSM-23[55]	ZSM-22[54]
Si/Al ratio bulk (NMR)	24	44	55	54
Si/Al ratio surface (XPS)	24	29	36	24
B.E.T. surface area (m^2/g)	101	165	273	256
Micropore volume (*t*-plot method) (μL/g)	34	52	97	96
External surface area (*t*-plot method) (m^2/g)	28	53	61	49

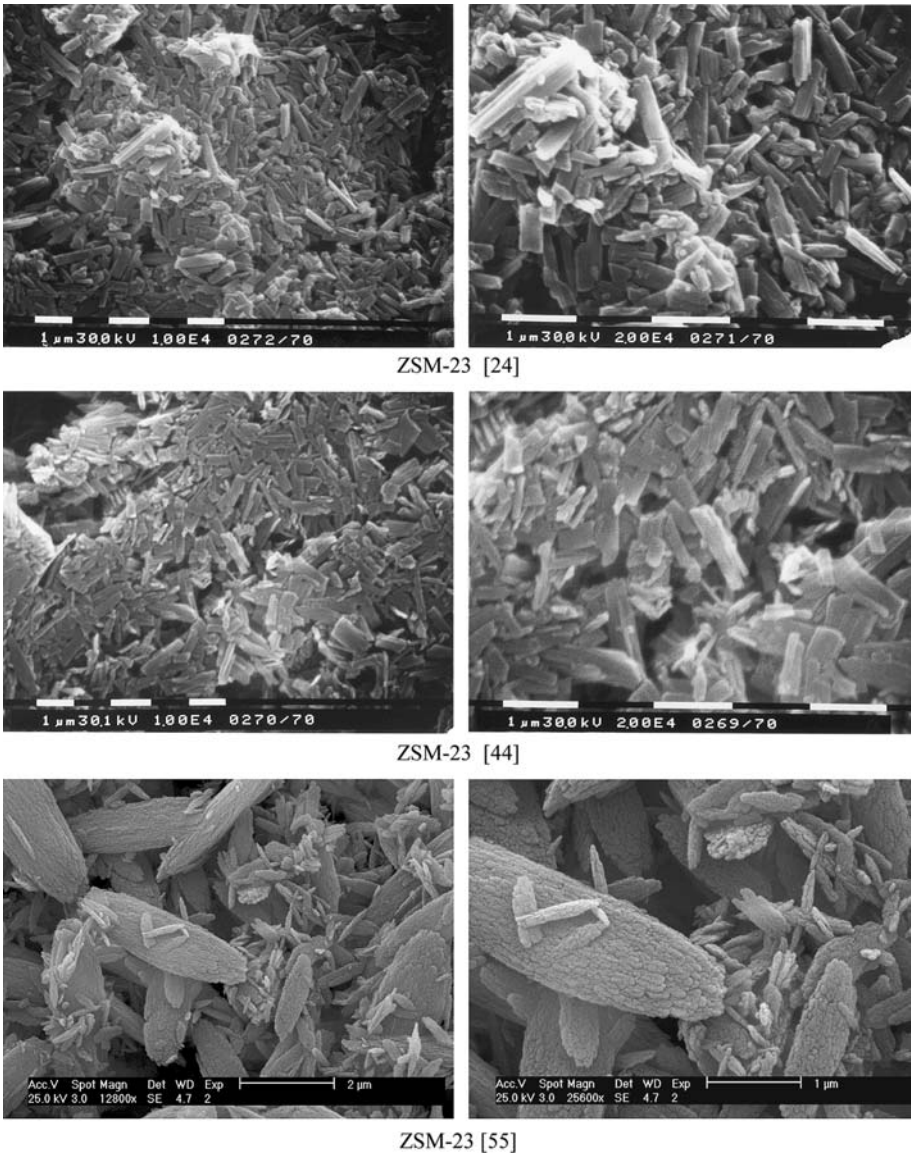

Figure 1. SEM images of ZSM-23[24], ZSM-23[44] and ZSM-23[55].

drally coordinated aluminum was virtually absent. The Al contents were quantified using the ZSM-23[24] sample for which the Al content was determined by chemical analysis as reference (table 1).

XPS was performed with a SSI X-probe (SSX-100/206) spectrometer from Surface Science Instrument working with a monochromatic Al Ka radiation (10 kV, 22 mA). Charge compensation was achieved by using an electron flood gun adjusted at 8 eV and placing a nickel grid 3.0 mm above the sample. Pass energy for the analyzer was 50 eV and the spot size was 1000 μm in diameter, corresponding to a FWHM (full width at half maximum) of 1.1 eV for the Au 4f7/2 band of a gold standard. The Si/Al ratios determined with XPS representative of the external surface are listed in table 1. In the ZSM-23[24] sample the Si/Al ratio in the bulk and on the external surface is the same, viz. 24. In the ZSM-23[44] and -[55] samples, and in the ZSM-22 reference

sample, the surface is enriched with Al compared to the bulk.

Ammonium exchanged ZSM-23 powder was impregnated with tetramine platinum (II) chloride, dissolved in a minimum amount of water to obtain a Pt loading of 0.3 wt%, and dried in air at 60 °C. The powders were compressed into a solid disc, crushed and sieved and the 300–500 μm pellet fraction retained for the catalytic experiments.

2.2. Catalytic experiments

The zeolite pellets were loaded in a stainless steel reactor tube with internal diameter of 1 cm and fixed between two plugs of quartz wool. The catalyst activation procedure comprised calcination under flowing oxygen at 400 °C followed by reduction in hydrogen at the same temperature. The feedstock for the catalytic experiments was a mixture of 2 wt% octadecane (Janssen, purity >99%) diluted with heptane (Janssen, technical grade, 99%). The total pressure in the reactor was 0.45 MPa and the temperature 230 °C. The hydrogen to hydrocarbon molar ratio in the feed was 13. Contact times of octadecane were up to 14,000 kg s/mol. The hydrocarbon was fed by a HPLC pump from a reservoir into a vaporization chamber, mixed with hydrogen and passed in downflow direction over the fixed catalyst bed. Analysis of the reaction products was done on-line using capillary GC. The identification of C_{18} skeletal isomers was reported earlier [7]. Under the applied reaction conditions, there was no conversion of heptane detected.

3. Results

Plots of the *n*-C_{18} conversion against contact time on Pt/ZSM-23[24], Pt/ZSM-23[44], Pt/ZSM-23[55] and Pt/ZSM-22[54] catalyst are reported in figure 2. The activity differences are not very pronounced. The activity order corresponds to:

$$\text{Pt/ZSM-22[54]} = \text{Pt/ZSM-23[24]} = \text{Pt/ZSM[55]} > \text{Pt/ZSM-23[44]}$$

The yield curves of isomers in total, monobranched isomers, dibranched isomers and cracked products on the three catalysts in the conversion range 65–100% are shown in figure 3. On all catalysts, isomer yields exceeding 60% were obtained. At a same conversion level, the yield of total isomers, monobranched isomers and dibranched isomers is lower on Pt/ZSM-23[24] and -[44] samples compared to Pt/ZSM-22[54]. Lower isomer yields are linked with higher cracking yields. The evolution with conversion of the yield of the different product fractions on Pt/ZSM-23[55] and Pt/ZSM-22[54] samples are very similar.

Gas chromatograms and peak assignments of mono- and multibranched isomers obtained with the ZSM-23 and −22 reference catalyst at *ca.* 25% multibranching yield are reported in figure 4. The chromatograms of *iso*-octadecanes obtained with the three ZSM-23 samples are almost identical. In comparison to the products obtained with ZSM-22 catalyst, there are some specific differences in the peaks of dibranched isomers. The relative intensities of the R and Q peaks, and of the O and N peaks are systematically different.

The distribution of the monobranched skeletal isomerization products at specific yield levels is presented in figure 5. The traces of ethylhexadecanes formed were not included in the distributions. The product distribution according to methyl positions in

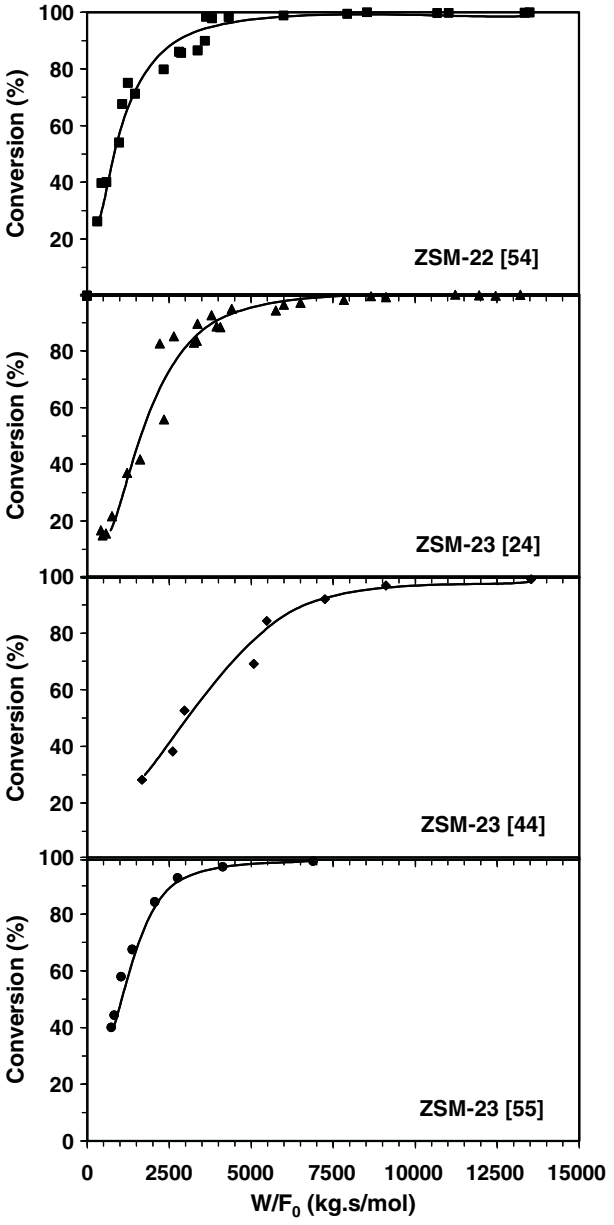

Figure 2. Octadecane conversion (%) against space time (kg s/mol) on ZSM-22[54], ZSM-23[24], ZSM-23[44] and ZSM-23[55] type catalysts.

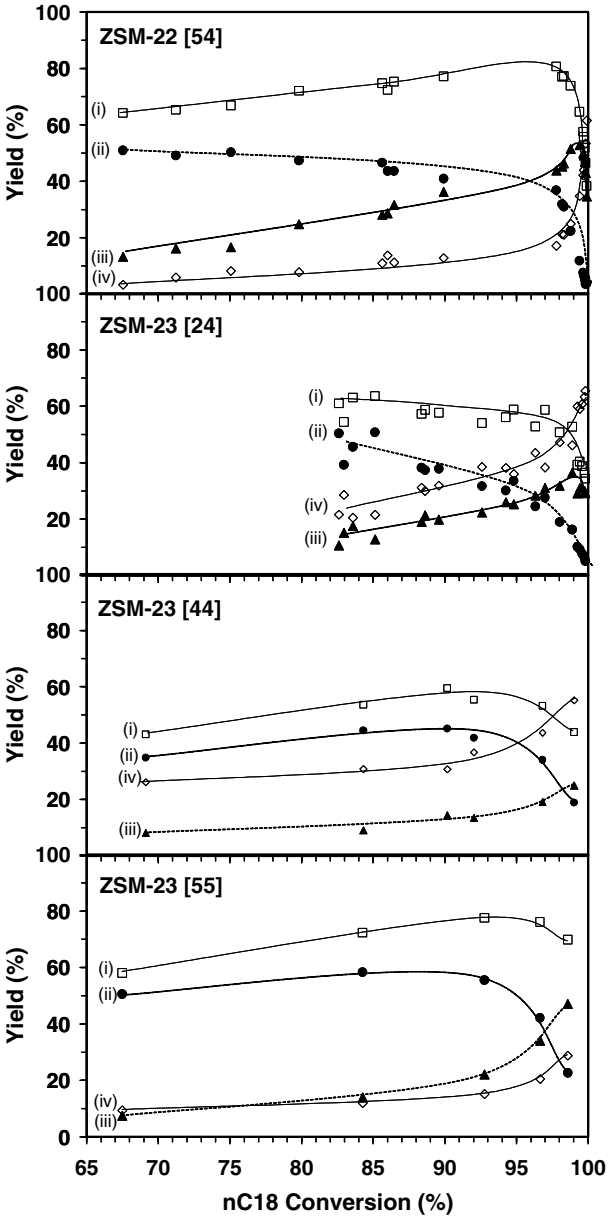

Figure 3. Yield of isomers in total (i), monobranched isomers (ii), dibranched isomers (iii) and cracked products (iv) on ZSM-22[54], ZSM-23[24], ZSM-23[55] and ZSM-23[44] against conversion (%).

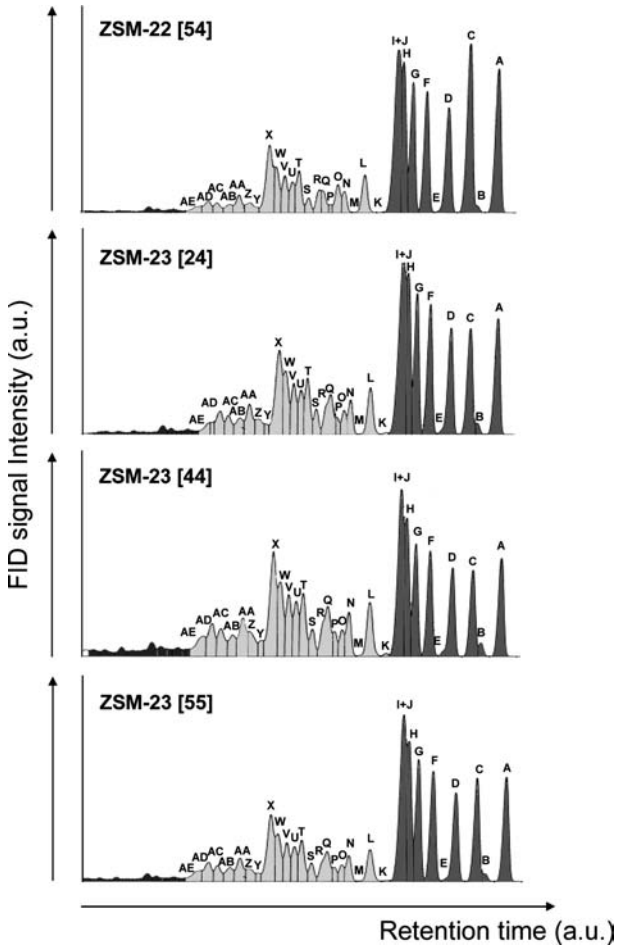

Figure 4. Comparison of chromatograms at approximately 25% monobranched isomerization yield on ZSM-22 and ZSM-23 type catalysts. Product identification: (A) 3-methylheptadecane; (B) 3-ethylheptadecane; (C) 2-methylheptadecane; (D) 4-methylheptadecane; (E) 4-ethylheptadecane; (F) 5-methylheptadecane; (G) 6-methylheptadecane; (H) 7-methylheptadecane; (I) 8-methylheptadecane; (J) 9-methylheptadecane; (K) methylethylpentadecane; (L) 2,14-dimethylhexadecane; (M) methylethylpentadecane; (N) 3,13-dimethylhexadecane; (O) 2,15-dimethylhexadecane; (P) 3,12-dimethylhexadecane; (Q) 4,13-dimethylhexadecane; (R) 3,11-dimethylhexadecane + 2,13-dimethylhexadecane; (S) 3,10-dimethylhexadecane; (T) 2,12-dimethylhexadecane; (U) 3,9-dimethylhexadecane; (V) 2,11-dimethylhexadecane; (W) 2,10-dimethylhexadecane; (X) 2,9-dimethylhexadecane + 2,8-dimethylhexadecane; (Y) 4,11-dimethylhexadecane; (Z) 4,10-dimethylhexadecane + 4,9-dimethylhexadecane; (AA) 4,8-dimethylhexadecane; (AB) 7,10-dimethylhexadecane; (AC) 5,11-dimethylhexadecane; (AD) 5,10-dimethylhexadecane + 5,9-dimethylhexadecane + 5,8-dimethylhexadecane; (AE) 6,10-dimethylhexadecane + 6,9-dimethylhexadecane.

methylheptadecanes on the three ZSM-23 samples is very similar. On the ZSM-22 sample, the yields of 2- and 3-methylheptadecane are higher than on ZSM-23, and the yields of 5-, 6-, 7-, 8- and 9-methylheptadecanes lower. When increasing conversion, the methylheptadecane distributions on the four catalysts evolve towards a same distribution, reflecting evolution toward the internal thermodynamic equilibrium of the methylheptadecane isomers.

Distributions of the dimethylhexadecane reaction products obtained on the four zeolite samples at 13% and 25% multibranching isomerization are given in table 2a and b, respectively. The product distribution of the three ZSM-23 samples are in very good agreement and differ from the distribution on the ZSM-22 sample. The 2,*n*-dMe–C16 and 3,*n*-dMe–C16 isomers are most abundantly formed on all zeolite samples but the preference for formation of 2,*n*-dMe–C16 isomers, and 2,15-dMe–C16 in particular, is less pronounced on the ZSM-23 zeolites. On both zeolites, the preferred position for the second branching in the 2,*n*-dMe–C16 family is located at carbon atoms in the range C8–C15.

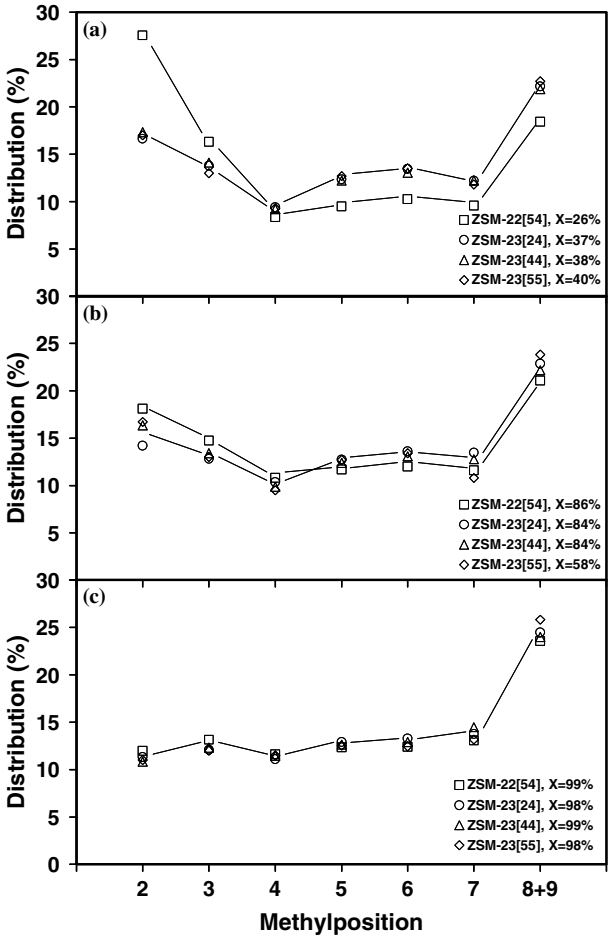

Figure 5. Distribution of monobranched isomers at increased conversion for ZSM-22[54], ZSM-23[24], ZSM-23[44] and ZSM-23[55] type catalysts: 20% monobranching yield (A); 45% monobranching yield (B); 19% monobranching yield (C) and the indicated conversion levels (*X*).

The most abundant isomers among the 3,*n*-dMe–C16 isomer family have their second branching in the range C9–C14. The minimum spacing of the branchings in the most favored isomers thus corresponds to five carbon atoms. In the 4,*n*-dMe–C16 isomer family, the formation of 4,8- and 4,13-dMe–C16 is favored, in particular on the ZSM-23 samples. The ZSM-23 samples also yield a higher amount of 5,*n*-dMe–C16 isomers compared to the ZSM-22 sample. The 6,*n*-dMe–C16 and 7,*n*-dMe–C16 isomers were formed in minor amounts on all catalysts.

4. Discussion

On bifunctional catalysts, skeletal branching occurs one branching at the time [23]. Multibranched skeletal isomers are more susceptible to cracking than monobranched isomers and the linear alkane. This reaction scheme is reflected in the yield curves of monobranched, dibranched and total isomers exhibiting a maximum when plotted against conversion (figure 2). The three ZSM-23 samples and the ZSM-22 catalysts all show high yields of isomers, exceeding 60%, illustrating their potential as isodewaxing catalysts. The distribution of monobranched and dibranched isomers obtained on ZSM-22 zeolite is significantly different from that obtained in a large pore zeolite such as ultrastable *Y* zeolite, where all reaction pathways are available to the molecule because of the absence of sterical hindrance. The present work reveals that although the detailed skeletal isomer distributions of ZSM-22 and ZSM-23 zeolites are quite similar, systematic deviations exist.

The investigated ZSM-23 samples present a significant variation in bulk and surface Si/Al ratio, particle size and microporosity (table 1). These differences lead to differences in catalytic activity (figure 2) and isomer yield curves (figure 3), but not to differences in skeletal isomer distributions (figures 4 and 5, and tables 2 and 3). It is concluded that framework topology is the predominating parameter determining for the positional branching selectivity of the zeolite. Some authors attributed the special branching patterns to differences in diffusivity of the respective isomers [10,12–14]. According to such model of product diffusion, acid site concentration, microporosity and particle size all should alter the product distributions. Our experimental results disprove the occurrence of such mechanism.

A careful examination of these skeletal isomer distributions and comparison with predictions from product diffusion models leads to additional contradictions. The methylheptadecane product distribution from octadecane conversion over the ZSM-22 is bimodal with methyl branchings at C2 and C5–C9 being preferred. Webb *et al.* [13] calculated a minimum in the diffusivity of the methylbranched isomers of decane and hexadecane for the methylbranching at C4, which they ascribed to structural features in the zeolite framework that provide a unique hindrance to molecular motion of specific molecules. The minimum at C4 in the distribution of monomethylbranched isomers obtained on ZSM-22 is then in agreement with product diffusion selectivity [10]. Modeling of diffusion in ZSM-23 revealed a monotonically decrease in the diffusivity of the isomers of 2M > 3M > 4M > 5M [12]. The experimentally obtained distribution of methylbranched skeletal isomers presented in this work reveals a preferential formation of isomers branched at C5 over C4 (figure 5).

The bimodal distribution of monomethylbranched isomers can be explained by invoking pore-mouth and key–lock catalysis. Skeletal branching near the end of the chain occurs when the molecule is adsorbed according to the pore-mouth mode. Branching at C5–C9 positions occurs when the molecule is adsorbed in key–lock mode, as proposed earlier for ZSM-22. The differences between the positional selectivity of methylbranching should be a result of the differences in

Table 2
Distribution of the multibranched isomers of octadecane at *ca.* 13% (A) and 25% (B) yield of multibranched isomers over ZSM-22[54], ZSM-23[24], ZSM-23[44] and ZSM-23[55] type catalysts

A	ZSM-22[54] $X(\%) = 67.5$ $Y_{multi}(\%) = 13.2$	ZSM-23[24] $X(\%) = 85.1$ $Y_{multi}(\%) = 12.9$	ZSM-23[44] $X(\%) = 92.0$ $Y_{multi}(\%) = 13.5$	ZSM-23[55] $X(\%) = 84.3$ $Y_{multi}(\%) = 13.9$
methylethylpentadecane	0.0	0.0	0.0	0.1
2,14-dimethylhexadecane	10.7	9.2	10.1	9.0
methylethylpentadecane	0.0	0.0	0.0	0
3,13-dimethylhexadecane	3.7	5.4	6.1	5.6
2,15-dimethylhexadecane	10.2	4.4	4.4	4.2
3,12-dimethylhexadecane	0.9	3.1	3.7	3.0
4,13-dimethylhexadecane	4.1	6.6	7.7	7.5
3,11-dimethylhexadecane				
2,13-dimethylhexadecane	4.3	2.5	2.5	2.3
3,10-dimethylhexadecane	2.4	2.5	2.6	3.0
2,12-dimethylhexadecane	9.6	7.7	7.8	7.8
3,9-dimethylhexadecane	5.2	5.6	5.6	5.3
2,11-dimethylhexadecane	8.0	7.4	7.8	7.5
2,10-dimethylhexadecane	9.7	8.7	9.5	9.3
2,9-dimethylhexadecane				
2,8-dimethylhexadecane	19.6	16.3	15.9	16.2
4,11-dimethylhexadecane	0.0	1.4	0.3	0.9
4,10-dimethylhexadecane				
4,9-dimethylhexadecane	1.8	1.4	1.6	1.6
4,8-dimethylhexadecane	3.3	4.2	4.0	4.2
7,10-dimethylhexadecane	1.4	3.0	1.9	3.1
5,11-dimethylhexadecane	1.5	3.5	2.5	2.8
5,10-dimethylhexadecane				
5,9-dimethylhexadecane				
5,8-dimethylhexadecane	2.3	4.6	3.9	4.9
6,10-dimethylhexadecane				
6,9-dimethylhexadecane	1.3	2.6	2.2	1.8

B	ZSM-22[54] $X(\%) = 79.8$ $Y_{multi}(\%) = 24.8$	ZSM-23[24] $X(\%) = 94.8$ $Y_{multi}(\%) = 25.3$	ZSM-23[44] $X(\%) = 99.0$ $Y_{multi}(\%) = 25.0$	ZSM-23[55] $X(\%) = 93.0$ $Y_{multi}(\%) = 22.0$
methylethylpentadecane	0.0	0.2	0.3	0.2
2,14-dimethylhexadecane	9.7	8.4	8.9	7.8
methylethylpentadecane	0.0	0.0	0.0	0
3,13-dimethylhexadecane	4.6	5.6	5.9	4.5
2,15-dimethylhexadecane	6.6	3.2	3.1	3.7
3,12-dimethylhexadecane	1.1	2.3	2.6	2.0
4,13-dimethylhexadecane	4.3	6.5	6.9	6.5
3,11-dimethylhexadecane				
2,13-dimethylhexadecane	4.6	3.1	3.0	2.7
3,10-dimethylhexadecane	2.7	3.1	2.7	3.5
2,12-dimethylhexadecane	9.6	8.7	8.3	8.4
3,9-dimethylhexadecane	6.4	6.6	6.7	5.6
2,11-dimethylhexadecane	8.1	7.6	7.4	7.3
2,10-dimethylhexadecane	10.4	9.6	9.5	9.3
2,9-dimethylhexadecane				
2,8-dimethylhexadecane	18.7	16.7	16.0	16.2
4,11-dimethylhexadecane	0.0	0.0	0.4	1.0
4,10-dimethylhexadecane				
4,9-dimethylhexadecane	2.0	1.7	1.7	2.9
4,8-dimethylhexadecane	3.6	4.6	4.7	5.2
7,10-dimethylhexadecane	1.5	2.4	1.8	3.2
5,11-dimethylhexadecane	1.8	2.9	3.2	2.9
5,10-dimethylhexadecane				
5,9-dimethylhexadecane				
5,8-dimethylhexadecane	2.6	4.2	4.3	5.0
6,10-dimethylhexadecane				
6,9-dimethylhexadecane	1.7	2.6	2.7	1.9

contributions of pore mouth with respect to key–lock catalysis between ZSM-22 and ZSM-23.

In the dimethylbranched isomer fraction obtained on ZSM-23, the minimum spacing between two methyl branches is five carbon atoms. As molecular models suggest that the bridge distances between neighboring pores are practically the same for ZSM-23 as for ZSM-22, this is in agreement with the results obtained on ZSM-22 and was explained in terms of key–lock catalysis in which the alkane adsorbs with two tails in adjacent pores. At this moment it is not possible to rationalize the details of the dimethylbranched isomer distributions. The extention of the kinetic model developed by Narasimhan *et al*. [17] for ZSM-22 to the ZSM-23 catalysts should make it possible to get a clearer view on the peculiar selectivities and selectivity differences on ZSM-22 and ZSM-23 catalysts.

5. Conclusions

In octadecane hydroisomerisation, ZSM-23 samples with different Si/Al ratios, microporosity and crystal size exhibit identical methyl- and dimethylheptadecane positional selectivities, different from ZSM-22. The branching selectivity is primarily determined by the framework topology, and much less by the acidity or crystal size. The finding suggests that product shape selectivity does not apply to octadecane isomerization on Pt/H-ZSM-23. Skeletal isomerization of octadecane on ZSM-23 is an example of pore-mouth and key–lock catalysis. The distribution of the positional methylheptadecane isomers is bimodal, with a minimum at C4, and maxima at C2 and at C5, C6, C7. Compared to ZSM-22, the preference for branching near the end of the chain is less pronounced on a ZSM-23. The distribution of methyl- and dimethylbranched skeletal isomers from octadecane is a fingerprint of a zeolite framework structure.

Acknowledgments

W.H. and J.F.M.D. acknowledge I.W.T. and F.W.O.-Vlaanderen for a Ph.D. and a postdoctoral fellowship, respectively. J.A.M. and P.A.J. acknowledge the Flemish government for supporting a concerted research action (G.O.A.). The involved teams participate in the IAP-PAI program [SC]2, sponsored by the Belgian government.

References

[1] S.J. Miller, in: *Zeolites and Related Microporous Materials: State of the Art*, eds. J. Weitkamp, H.G. Karge, H. Pfeifer and W. Holderich (Elsevier, Amsterdam, 1994).
[2] J.A. Martens and P.A. Jacobs, Zeolites 6 (1986) 334
[3] S. Ernst, J. Weitkamp, J.A. Martens and P.A. Jacobs, Appl. Catal. 48 (1989) 137
[4] R. Parton, L. Uytterhoeven, J.A. Martens, P.A. Jacobs and G.F. Froment, Appl. Catal. 76 (1991) 131
[5] J.A. Martens, W. Souverijns, W. Verrelst, R. Parton, G.F. Froment and P.A. Jacobs, Angew. Chem. Int. Ed. Engl. 34 (1995) 22
[6] M.C. Claude and J.A. Martens, J. Catal. 190 (2000) 39
[7] M.C. Claude, G. Vanbutsele and J.A. Martens, J. Catal. 203 (2001) 213
[8] V.T. Nghiem, G. Sapaly, P. Mériaudeau and C. Naccache, Top. Catal. 14 (2001) 131
[9] G. Sastre, A. Chica and A. Corma, J. Catal. 195 (2000) 227
[10] T.L.M. Maesen, M. Schenk, T.J.H. Vlugt, J.P. de Jonge and B. Smit, J. Catal. 188 (1999) 403
[11] P. Mériaudeau, V.A. Tuan, F. Lefebre, V.T. Nghiem and C. Naccache, Microporous Mesoporous Mater. 22 (1998) 435
[12] E.B. Webb III and G.S. Grest, Catal. Lett. 56 (1998) 95
[13] E.B. Webb III, G.S. Grest and M. Mondello, J. Phys. Chem. B 103 (1999) 4949
[14] M. Schenk, B. Smit, T.J.H. Vlugt and T.L.M. Maesen, Angew. Chem. 113 (2001) 758
[15] R.A. Ocakoglu, J.F.M. Denayer, G.B. Marin, J.A. Martens and G.V. Baron, J. Phys. Chem. B 107 (2003) 398
[16] J.F. Denayer, A.R. Ocakoglu, W. Huybrechts, J.A. Martens, J.W. Thybaut, G.B. Marin and G.V. Baron, Chem. Commun. (2003) 1880.
[17] C.S.L. Narasimhan, J.W. Thybaut, G.B. Marin, P.A. Jacobs, J.A. Martens, J.F. Denayer and G.V. Baron, J. Catal. 220 (2003) 399
[18] W.M. Meier, D.H. Olson and Ch. Baerlocher, *Atlas of Zeolite Structure Types* 4 ed.(Elsevier, Amsterdam, 1996)
[19] J.A. Martens, M. Tielen, P.A. Jacobs and J. Weitkamp, Zeolites 4 (1984) 98
[20] S. Ernst, R. Kumar and J. Weitkamp, Catal. Today 3 (1988) 1
[21] S. Ernst, G.T. Kokotailo, R. Kumar and J. Weitkamp in: *Proceedings 9th International Congress on Catalysis*, eds. M.J. Phillips and M. Ternan, (The Chemical Institute of Canada, 1988).
[22] S. Ernst, J. Weitkamp, J.A. Martens and P.A. Jacobs, Appl. Catal. 48 (1989) 137
[23] J.A. Martens and P.A. Jacobs, in: *Theoretical Aspects of Heterogeneous Catalysis*, eds. J.B. Moffat (Van Nostrand Reinhold, New York, 1990).